



Deliverable Number: **D 20.3.1.x**
Deliverable Title: **Report on low background solid-sample high -
pressure p-cell.**

Delivery date: **xx/xx/2012**
Leading beneficiary: Babeş-Bolyai University, Cluj-Napoca, ROMANIA
Dissemination level: Public
Status: final version
Authors: D. Andreica
D. Marconi
R. Khasanov
A. Maisuradze
A. Amato

Project number: 226507
Project acronym: NMI3
Project title: Integrated Infrastructure Initiative for Neutron Scattering and
Muon Spectroscopy
Starting date: 1st of February 2009
Duration: 48 months
Call identifier: FP7-Infrastructures-2008-1
Funding scheme: Combination of CP & CSA – Integrating Activities

Abstract

Pressure, together with temperature and magnetic field, is an important parameter for the study of the phase diagram of materials. Under applied pressure, the interatomic distances shrink and the interactions between the atoms are modified leading to new and sometimes exotic physical properties, pressure induced phase transitions, or changes of the characteristic parameters (e.g. transition temperature) of the investigated materials.

In the following report, the requirements for a μ SR under pressure experiment, a brief history of the topic and selected experimental results obtained using the μ SR under pressure method are presented, including the new developments and limitations of the method.

Acknowledgements

The project is supported by the European Commission under the 6th Framework Programme through the Key Action: Strengthening the European Research Area, Research Infrastructures. Contract n°: RII3-CT-2003-505925

Document History

Version	Modification	Date	Author(s)

JRA: Technologies for μ SR at high pressures - report

D. Andreica¹, D. Marconi¹, R. Khasanov², A. Maisuradze², A. Amato²

¹Babeş-Bolyai University, Faculty of Physics, Cluj-Napoca, ROMANIA

²Laboratory for Muon Spin Spectroscopy, Paul Scherrer Institute, Villigen, SWITZERLAND.

1. Introduction.

Pressure, together with temperature and magnetic field, is an important parameter for the study of the phase diagram of materials. Under applied pressure, the interatomic distances shrink and the interactions between the atoms are modified leading to new and sometimes exotic physical properties, pressure induced phase transitions, or changes of the characteristic parameters (e.g. transition temperature) of the investigated materials.

Pressure p on a surface S is obtained by applying a certain force F on and perpendicular to that surface and it is calculated using: $p = F/S$. Usually, for the scientific use, pressure (force) is not applied directly to the sample, with the exception of the case when uniaxial pressure is needed. Commonly, one makes use of Pascal's law to apply pressure on a fluid where the sample is immersed, obtaining a so called hydrostatic pressure i.e. the sample is squeezed uniformly from all directions.

Our goal was to design and build pressure cells capable of sustaining high hydrostatic pressures, for the use in μ SR experiments with different sample environments (temperature and magnetic fields). The design of such pressure cells, including the choice of material, is strongly influenced by the specific characteristics of the μ SR experiment and by the sample environment available. These parameters will be detailed in the following sections of the report.

In this section, a short description of the μ SR method is provided, in which the specificity of the combination pressure – μ SR (large bulky samples) is emphasized. A brief history of the μ SR under pressure method is then presented, along with new developments in the area. The choice of materials (for the p-cell, piston, liquid for transmitting pressure) will be discussed together with the design of the p-cells and the method for measuring the pressure at low temperature. At each stage of the discussion, information regarding scientific achievements and goals are detailed.

2. The μ SR method.

The possible use of muons for the investigation of matter was predicted by the particle physicists L.R. Garwin and coworkers in 1957 in their article “Observations of the Failure of Conservation of Parity and Charge Conjugation in Meson Decays: the Magnetic Moment of the Free Muon” [GA57] where they wrote: “It seems possible that polarized positive and negative muons will become a powerful tool for exploring magnetic fields in nuclei, atoms, and interatomic regions”.

The regular use of positive muons (elementary particles with charge e^+ , spin $1/2$ and lifetime $\cong 2.2 \mu\text{s}$) for the study of the magnetic properties of materials began in the beginning of the 70’s, using the muons created from pions via nuclear reactions at the existent accelerators at that time. Now, there are only four “muon factories” available around the world: in Switzerland (PSI), in the UK (ISIS), in Canada (TRIUMF) and in Japan (J-PARC).

In a usual μ SR experiment, polarized positive muons μ^+ , are implanted (and give a start signal for a clock) into the sample, where they precess around the local magnetic field at the place where they come at rest, the muon site. The μ^+ decays by emitting a positron (which gives a “stop clock” signal), preferentially along the muon spin at the moment of the decay. The decay of the muons recorded in $N(t)$ histograms on different directions, contains valuable information about the magnitude and dynamics of the magnetic field at the muon site. The recorded histograms are usually fitted using:

$$N(t) = B + \frac{N_0}{t_\mu} \exp(-t/t_\mu) (1 + A_0 P(t))$$

where B is a constant accidental background, t_μ is the μ^+ lifetime A_0 is the so called asymmetry or amplitude of the signal, and $P(t)$ is the time evolution of the projection of the polarization of the muon ensemble along the direction of the observation (positron counter). $A_0 P(t)$ is called μ SR spectra and contains the information about the physics of the sample. One should keep in mind that this term is “summative”, in the sense that:

$$A_0 P(t) = \sum_i A_i P_i(t) \text{ with } A_0 = \sum_i A_i$$

i.e. muons “seeing” different magnetic environments will have a different signature in the final μ SR spectra. This is very useful/important information also for the analysis of μ SR spectra of samples inside pressure cells. In that case:

$$A_0 P(t) = A_{p-cell} P_{p-cell}(t) + A_{sample} P_{sample}(t) \text{ with } A_0 = A_{p-cell} + A_{sample}.$$

The value of A_0 can be easily obtained from a calibration run performed in weak transversal magnetic field (with respect to the initial muon polarization) at a temperature at which the sample is in the paramagnetic phase. At this temperature, the average field at the muon site is the applied field, thus all the muons will turn around the “same” transverse field and $P(t)$ is a damped oscillation with full asymmetry (because of the field distribution/dynamics at the muon site), see the simulation (black dots) presented in Figure 1. The spectra was fitted using

$$P(t) = \cos(\gamma B_{loc} t) * \exp(-\lambda t)$$

Where $\gamma = 2 \cdot \pi \cdot 0.01355$ MHz/G, $B_{loc} = 50$ G and $\lambda = 0.1$ (μ s) $^{-1}$

A damped oscillation is also expected from the μ SR spectra recorded for muons stopped in a magnetic sample (sample at a temperature below its magnetic transition temperature), in zero applied external magnetic field and if all the muon sites are magnetically equivalent. In that case the local field is created by the surrounding electronic magnetic moments (external field = 0) and the asymmetry of the oscillating component is 2/3 of the total sample asymmetry. The rest of 1/3 of the total sample asymmetry will only show an

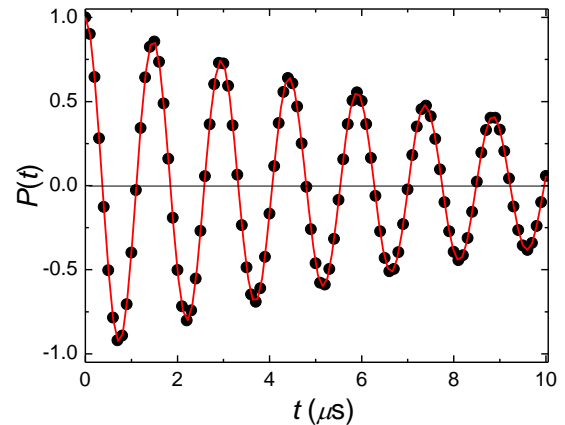


Figure 1. $P(t)$ for a weak transversal field (wTF, 50 G) calibration experiment.

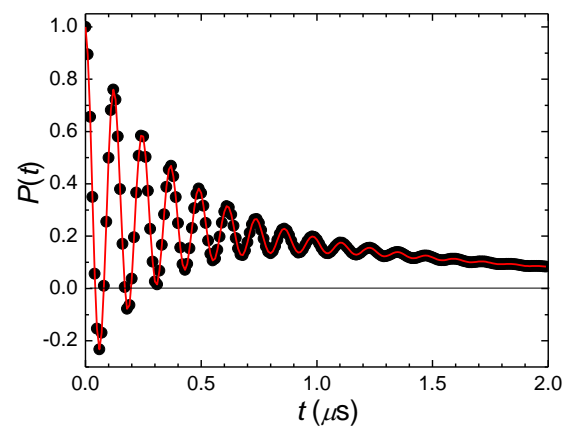


Figure 2. $P(t)$ for muons stopped in a magnetic sample (see text).

exponential relaxation. This is because on average 1/3 of the muon will “see” a local field parallel to their initial polarization and they will not precess, while the rest of 2/3 of the muons will “see” local fields perpendicular to their initial polarization i.e. precession of the muon and oscillations in the μ SR spectra. An exponential relaxation of the 1/3 term is observed if there is field dynamics perpendicular to the initial muon polarization since it can induce transitions between the muon states. For the example spectra presented in Figure 2, the following fitting function was used:

$$P(t) = \frac{2}{3} \cos(\gamma B_{loc} t) * \exp(-\lambda t) + \frac{1}{3} \exp(-\lambda_1 t)$$

where $B_{loc} = 600$ G, $\lambda = 3$ (μ s)⁻¹ and $\lambda_1 = 0.7$ (μ s)⁻¹. Compare the time scales in Figure 1 (paramagnetic sample in wTF) and Figure 2 (magnetic sample).

For the “classic” μ SR experiments, surface muons (obtained from the pions decaying at rest near the surface of the production target) are used. They are monochromatic, with a μ^+ momentum of 29.8 MeV/c (energy of 4.1 MeV) and can be stopped in thin samples of about 160 – 200 mg/cm².

If we want that the muons to reach samples inside pressure cells, their energy should be much larger and one uses a high energy muon beam (obtained from pions that leave the target at high energy). The polarization of the high energy muon beam, in the laboratory frame, is about 80%. By tuning the muon momentum, one can choose the optimum value which maximizes the ratio between the number of muons stopped inside the sample to the number of the muons stopped inside the pressure-cell (signal to “noise” ratio). This ratio depends not only on the muon momentum (Figure 3) but also on the width of the muon beam (Figure 4).

For a correct calculation of the ratio (as described in the legend of Figure 3) one should also keep in mind that the beam profile is Gaussian (see Figure 6 for a scan of the muon beam, perpendicular (horizontal and vertical) to the beam direction) i.e. there are more muons in the center of the beam compared to the edges. Why do only the blue and red lines count, independent of the width of the muon beam? Because the muons that pass through the p-cell without stopping or nearby the p-cell without touching it can be eliminated from the μ SR spectra using a common veto system based on the coincidence between the start – stop signals.

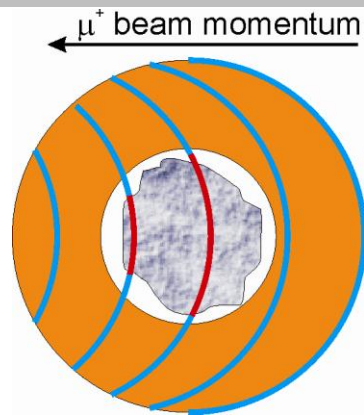


Figure 3. Stopping of the muons inside the pressure cell (blue line) and sample (red line) for different values of the μ^+ momentum (transversal section of a piston-cylinder pressure – cell, the sample, grey colour, is in the center). The width of the beam was chosen to be larger than the width of the p-cell. The optimum value of the momentum maximizes the ratio between the length of the blue line and that of the red line i.e. the ratio between the number of muons stopped inside the sample and the number of muons stopped inside the p-cell.

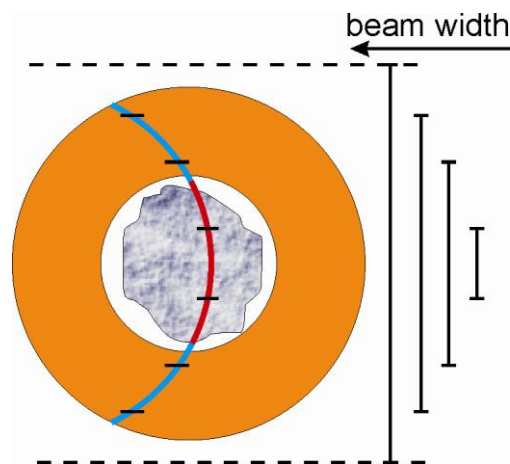


Figure 4. For the optimum muon momentum (see Figure 3), this picture displays the spatial dependence of the muon stops inside the pressure cell (blue line) and sample (red line) for different values of the beam width (beam spot diameter).

Unfortunately, as described below, the diameter of the muon beam cannot be decreased indefinitely. Moreover, the diameter of the muon beam (for the same settings of the beam window) depends also slightly on the muon momentum. Obtaining the best settings for the experiment i.e. the optimal values of the beam momentum is therefore a tricky operation.

Further refinements of the calculation need to take into account the dispersion of the beam momentum, convoluted with the “natural” longitudinal and transversal dispersion of the beam when crossing the walls of the cryostat, the p-cell walls and the sample. These last effects are of the order of a few millimeters, see Figure 5, and limit the minimum possible dimension of the beam spot at the sample.

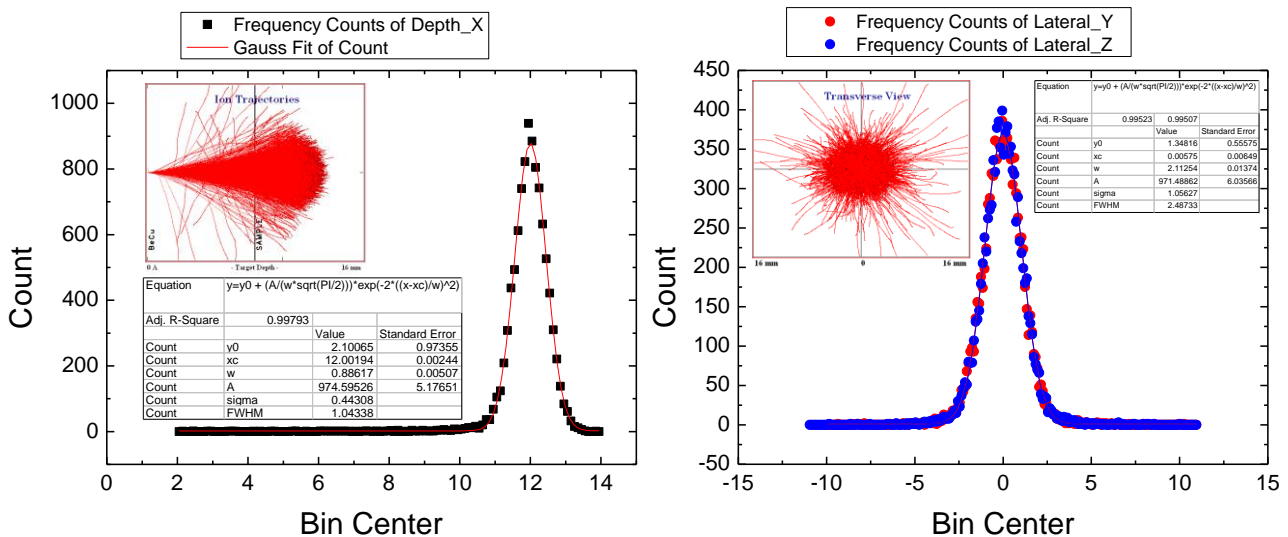


Figure 5. Left: simulation of the range; right: lateral straggle of muons in the sample (Ni in this case). The calculations were performed using the SRIM-2008 package. The simulation was for an 8 mm wall (Cu-Be) followed by an 8 mm sample (Ni). The incoming energy of the muons was chosen such that they stop with a large probability in the center of the 8 mm Ni sample.

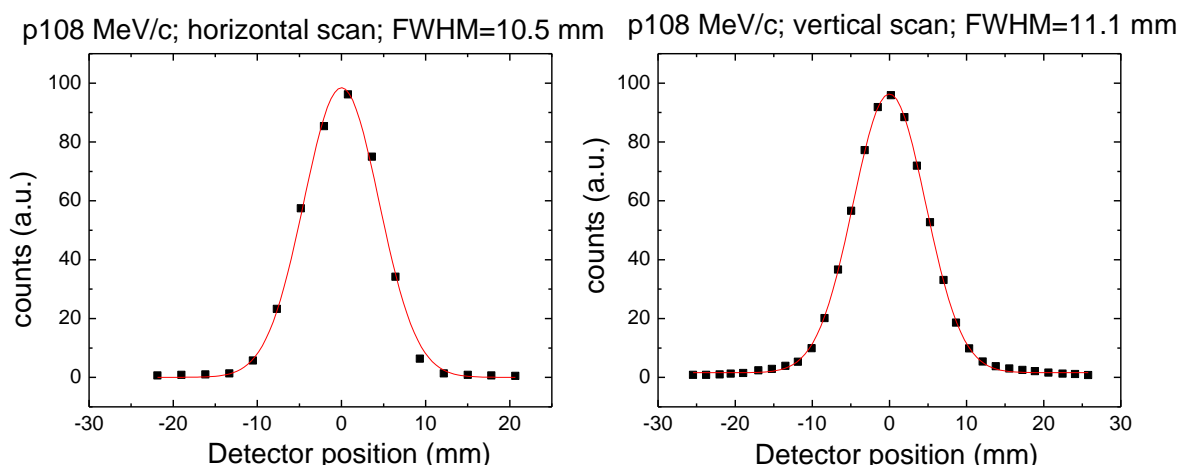


Figure 6. Gaussian distribution of the muon beam measured on two directions perpendicular to the beam, using a 1 cm² scintillator and a Ø 8 mm collimator. These measurements were further confirmed by using a Nikon D90 photo camera (not shown here). Beam profile at half intensity could be reduced to 5x9 mm by using a 4x10 collimator. Measurements were performed out of the cryostat.

In summary:

- Large sample dimensions are required in order to give a reasonable signal from the sample inside the p-cell. This is a particularity of μ SR, in comparison with other types of measurements: resistivity, magnetic, specific heat, etc. where samples of less than one mm can be measured thus allowing the use of diamond anvil cells & co.

- The piston cylinder pressure cell provides a reasonable sized cavity for the sample and is therefore a good choice for μ SR experiments for the time being.. Therefore, the entirety of our work was dedicated to improving the characteristics of this type of pressure cell for use in the existing cryogenic environment (maximum outer diameter of the p-cell has to be about 24 mm).
- One can get more than 50% of the muons stopped inside the sample if using a piston-cylinder pressure-cell with \varnothing 7 mm sample space or about 30% if using a pressure-cell with \varnothing 5 mm sample space. On the other hand, as it will be shown below, a \varnothing 7 mm p-cell can sustain less pressure than a \varnothing 5 mm one. Thus, the choice of the p-cell will be dictated by the maximum pressure required and by the complexity of the μ SR signal.
- After choosing the type of p-cell for the experiment, the optimization of the beam optics (beam calibration) is the first and one of the most important steps when performing a μ SR under pressure experiment.

We should not end this chapter without mentioning that a test on the possible use of anvil pressure cells in μ SR experiments was performed at PSI [MA11]. A 5 x 4.5 x 3 mm dense hematite sample was placed in between two \varnothing 5 mm Boron-Nitride anvils (similar anvils are used for reaching 10 GPa pressures). The measurements were performed at ambient pressure, outside of the cryostat. Beam momentum scans position calibrations have indicated that one can expect that about 20% of the muons will stop in the sample in the ideal case. This is quite a reasonable fraction if one is only interested in the pressure dependence of transition temperatures or when the μ SR signal is easy to fit. However, there are several caveats. Firstly, none of our cryostats can cool such a p-cell. Secondly, the remaining 80% of the muons stop in different parts of the p-cell creating possible fit problems and finally, the value of 20% is for 100% filling of the sample space.

3. Cylindrical p-cells for the use in μ SR under pressure experiments.

As described above, sample size and hydrostaticity of the pressure are key elements for the success of a μ SR under pressure experiment. It is quite essential that pressure is hydrostatic otherwise stress inside the sample can produce lattice defects which can trap muons and/or wide distributions of the internal field at the muon site.

In the following section, a short historical perspective is presented. Since almost all the important achievements were planned/obtained at PSI, for its high energy muon beam, we will stick to their presentation.

One of the first pressure cells used for μ SR experiments was a *clamped cell using oil as pressure transmitting media*, capable of reaching 7 kbar. It was used by Butz and co-workers for studying the pressure dependence of the local magnetic field at the muon site in transition metals Fe and Ni [BU80]. The drawback of this pressure cell was that at low temperatures the oil would freeze leading to non-hydrostatic conditions.

In order to provide the hydrostatic conditions and lower temperatures required for the magnetic study of the rare earth metals (which require also larger pressures), *a gas pressure cell was designed* [BU86, KR94], for use at pressure up to 14 kbar. Helium also solidifies at low temperatures/high pressures but it cannot support significant shear forces thus hydrostaticity is preserved. A sketch of the system is shown in Figure 7 [KA00]. Details of the construction can be found in [BU86, KR94]. Even if the designated pressure was 14 kbars, this pressure system (with pressure cells made of either CuBe or Ti) was able to withstand (due also to security reasons) only about 9 kbar for a 7 mm diameter / ~ 70 mm length of the sample space.

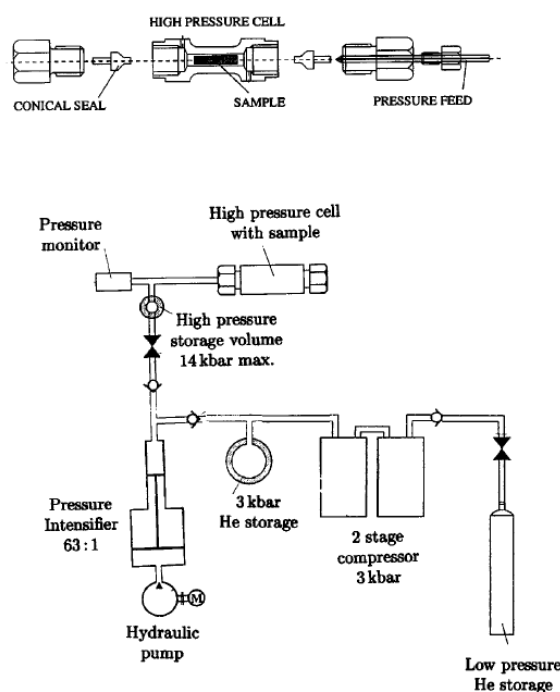


Figure 7. Schematic of the gas high pressure system [KA00].

This type of pressure device was successfully used up until 1999 for the study of elemental rare earth metals and for some intermetallic compounds: spin turning and critical behavior in elemental gadolinium under applied pressure [DE79, KR94, HA94, WA86, SC97]; pressure dependence of the contact field in Gd, Ho, Di [KA00, LI87]; the effect of the pressure on the T_N of (YTb)Mn₂ [SC99] and GdMn₂ [MA96, MA00]; the effect of lattice compression on the contact field of La₂CuO₄ [KA00] and the proof that μ SR under pressure works with a powder sample. The limitations in pressure and temperature (heavy

fermion systems could not be investigated because very low temperatures could not be reached), combined with security issues have led to a decrease in the level of interest in the use of such a pressure system.

At the beginning of 2001, lower temperatures and higher pressures could be obtained by using a *single layer piston cylinder pressure cell using liquid as pressure transmitting media*, see below [AN01], mounted on a Janis cryostat (2.2 K – 300 K) or on the cold head of a He3 cryostat (0.3 K – 300 K), enlarging the spectra of possible candidates for μ SR under pressure to strongly correlated electron systems, including heavy fermions.

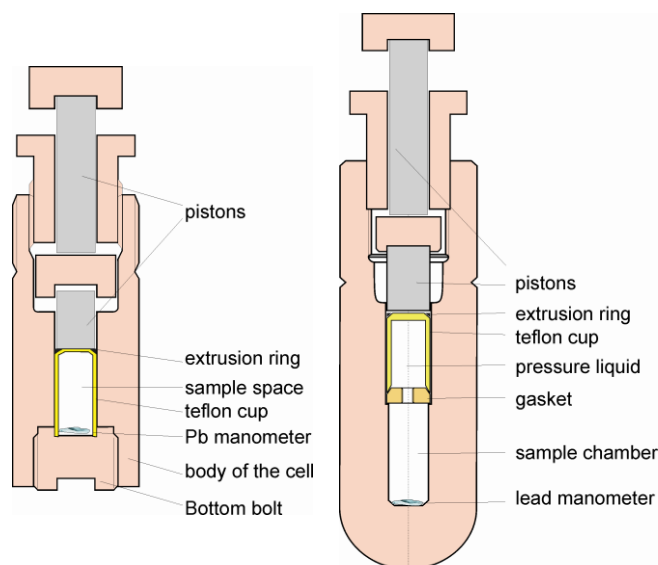


Figure 8. : left: “classic” single wall clamped p-cell opened at both ends; right: opened at one end.

The pressure cell used at that stage was a modification (Figure 8 - right) of a classic (Figure 8 - left) clamped pressure cell opened at both ends. The classical p-cell was modified because of the sample environment (at the beginning only the Janis cryostat was available) i.e. the distance between the center of the cryostat windows to the bottom of the sample space and the available inner diameter of the cryostat (27 mm) that the design of the pressure cell has changed. In addition, since the μ SR signal of the Teflon cup is not “neutral”, see below, the sample space was also modified [AN01] resulting in what is commonly denominated as a *PSI p-cell*. Initially, these p-cells were made out of a Cu-Be alloy and reach approximately 9 kbar (13-14 kbar) for a 7 mm (5 mm) inner diameter of the cell. Notably, the μ SR cells are long cylindrical cells, if we use the description given by Eremets in [ER96]. The use of MP35N improved the situation and pressures of 19-20 kbar could be achieved on a regular basis. All the pressures we are referring to here are pressures *measured* at low temperatures, not applied pressures at room temperature. These two values can differ significantly.

Also noteworthy, is that an MP35N p-cell opened at both ends was tested on a He3 cryostat for a while by a group from the Braunschweig University [KL-00] but its development was cancelled because of design/leak problems.

The latest developments are *double layers pressure cells* made of combinations of CuBe and MP35N. The dimension of the sample space limits the maximum pressure to 24 kbar for both a 6 mm MP35N/MP35N p-cell opened both sides and a 5 mm MP35N/MP35N PSI type p-cell. All these will be presented in more detail in chapter 5.

4. The scientific interest for μ SR under pressure experiments.

The μ SR – dedicated *p*-cells, have raised the interest of many scientists because they offered a new tool for the microscopic investigation of the physical properties of materials. At the beginning, the field of heavy fermion physics was mainly taken advantage from the use of this technique. Then studies were extended towards the investigation of frustrated magnetism, (new) superconductors, In the following we will present a few examples for the successful use of the mSR under pressure method.

a) Heavy fermions under pressure:

A so called concentrated Kondo system is a compound having the Kondo impurities (localized *4f* or *5f* magnetic moments, Ce, Yb or U) building up a regular lattice. At low enough temperatures, a narrow resonance in the density of states near the Fermi level is formed, due to the strong coupling between the conduction electrons and the localized *f* electrons. These states are described in terms of quasi-particles having enhanced effective mass (heavy fermions) due to the interaction with the other particles.

In the concentrated Kondo systems, there is a delicate competition/balance [DO77] between the inter-site RKKY interaction (which tends to drive the system towards a magnetic ground state) and an intra-site Kondo screening of the local moments by the conduction electrons (which pushes the system towards a nonmagnetic ground state). This balance is very sensitive to applied pressure because both interactions depend on the same parameter, the exchange coupling parameter between the localized and conduction electrons. At values of the pressure for which the magnetic ordering is suppressed (but not only), a plethora of interesting properties are observed (heavy fermions, spin-fluctuation-mediated superconductivity, non Fermi liquid behavior, quantum critical point (QCP), ...). Even though this is only a simplified view of the problem, it offers a good picture of the main interactions in these systems.

μ SR and μ SR under pressure was often employed for the investigation of heavy fermions because of their extreme sensitivity to small magnetic moment magnetism, phase separation issues (coexistence or competition between different phases) and electron spin dynamics. Examples are CeCu_2Si_2 [ST06], CeIn_2 [RO11], CeRhIn_5 [HE09], CeRhSi_3 [EG12], CeB_6 , hydrogenated CeNiSn , CePt_2In_7 , UGe_2 [SA10], URu_2Si_2 [AM03, AM04], UCoGe [VI09], to mention only the samples for which publications exist or are under scrutiny.

The interplay between magnetism and superconductivity is a topic of major interest and intense research. A QCP separates the nonmagnetic from the magnetic ground states [GE08, SI10, CO05] and quantum fluctuations determine the physical properties of such systems at low temperatures. Since the location and the nature of the QCP is important for understanding the interplay between superconductivity and magnetism, external pressure was employed quite often as a tuning parameter, driving the system through a QCP.

This was the case, for example, for CeRhSi_3 , a noncentrosymmetric heavy fermion antiferromagnet [KI07, MU98, MU07] suspected to display a QCP [KI07, TE07, TA10] under applied pressure. The relation between the QCP and the superconducting phase that shows up at low temperatures for pressures larger

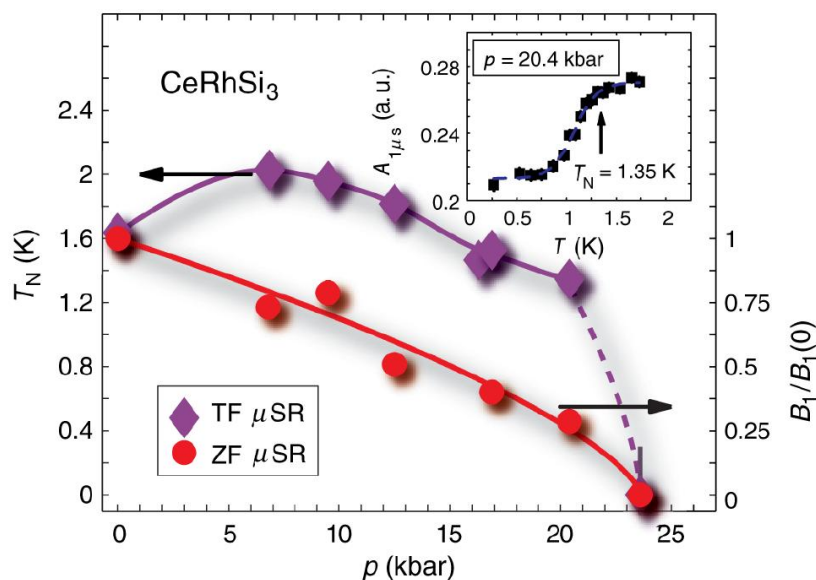


Figure 9 [EG12]. Pressure dependence of the Néel temperature (diamonds) and normalized internal field $B_1/B_1(0)$ (circles). The insert shows the result of a wTF temperature scan across the transition indicating the “loss” of the signal at the magnetic transition.

than 12 kbar [KI07, KI05] was also under debate. The μ SR under pressure experiments were performed up to 24 kbar and down to 0.27 K on a newly

developed (see below), double wall MP35N/MP35N pressure cell cooled in a He3 Cryostat [EG12]. The measured data suggest that the ordered moments are gradually quenched with increasing pressure and fully suppressed at 23.6 kbar. On the contrary, the Néel temperature shows a maximum at around 7 kbar and thus different pressure dependence, see Figure 9.

Examples of μ SR spectra recorded at pressures just below and above the QCP are presented in Figure 10. One can clearly observe, at 20.4 kbar and 0.27 K, the fast relaxing component at low time, characteristic of a magnetic ground state (compare with the spectra at the same pressure, at 1.76 K). There is no such behavior at 23.6 kbar and 0.27 K indicating that the ground state of CeRhSi₃ is no longer magnetic at this pressure.

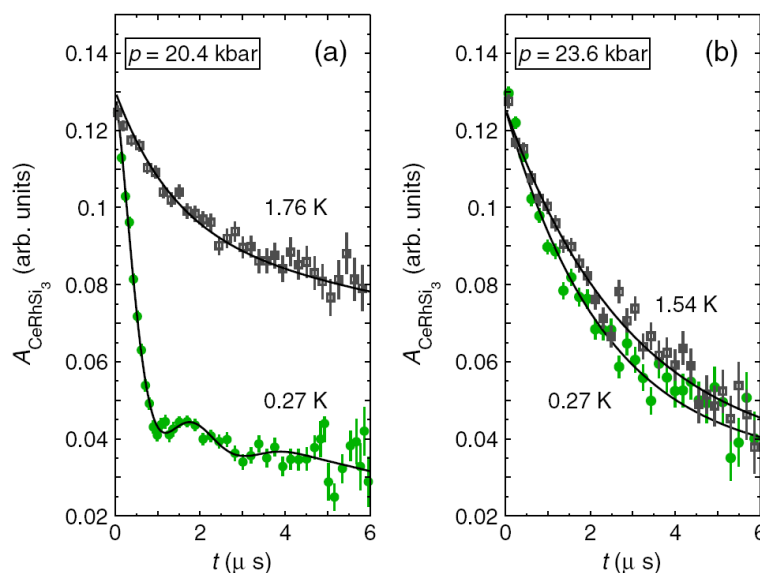


Figure 10 [EG12]. μ SR spectra recorded at (a) 20.4 and (b) 23.6 kbar at two different temperatures. The signal of the pressure cell was subtracted.

μ SR under pressure was also used as “problem solver” for different issues related to the physics of heavy fermions. For example, URu₂Si₂ was for long time, thought to have a second order phase transition below a temperature $T_0 = 17.5$ K [PA85], with a small ordered magnetic moment [BR87] that gradually increases with the applied pressure until about 13 kbar where there is a jump from 0.23 μ B to 0.4 μ B of the magnetic moment / U ion [AM99]. Careful μ SR under pressure experiments performed both on poly and single crystalline URu₂Si₂ samples have revealed a quite different picture [AM03, AM04]. First of all they have revealed the importance of sample quality and experimental conditions (pressure homogeneity and hydrostaticity). The 17.5 K transition (a “hidden order” transition, because the order parameter is unknown and still under debate) does

not involve any magnetism with small ordered moments, more precisely, the onset of magnetic ordering (with characteristic temperature T_M) occurs at low(er) temperatures only for pressures larger than 6 kbar i.e. the magnetism in URu_2Si_2 is induced by the applied pressure and it does not appear at T_o . The U magnetic moment (inferred from the frequency of the oscillations observed in the μ SR spectra as for Figure 10) is pressure independent above 6 kbar i.e. there is no gradual increase of the magnetic moment and no jump above 13 kbar (maximum pressure in the μ SR experiment was 14.5 kbar). The temperature dependence of the observed frequency clearly indicates a first-order transition between the hidden-order state and the magnetic state. By increasing the pressure, the onset temperature T_M is shifted to values similar to the hidden order temperature T_o . Once $T_M > T_o$ (pressures > 10 kbar) the hidden order phase disappears and the system undergoes a second order transition between the paramagnetic state and the ferromagnetic state.

Another typical example is the A/S (Antiferromagnetic/Superconducting) single crystalline $CeCu_2Si_2$: phase separation between the antiferromagnetic and superconducting region takes place before at low temperatures almost the whole crystal only displays superconductivity. Antiferromagnetism and superconductivity exclude each other in this crystal on a microscopic scale [ST06], see also [HI09] for the interplay between superconductivity and magnetism in $CeIrSi_3$.

Phase coexistence/separation issues were also addressed for other types of compounds: it was thought to exist in MnSi at high pressures [YU04, UE07]. MnSi is a weak itinerant ferromagnet which orders magnetically below 29 K, with a long period helical structure [WI66]. The magnetic transition temperature is suppressed by applying pressure (totally suppressed at about 15 kbar [TH89]).

Recent μ SR under pressure experiments [AN10] have shown that no magnetic phase separation is present in MnSi at low temperatures and, at the same time, emphasized the importance of pressure homogeneity and access to low temperatures for getting reliable information on the phase separation problem.

b) Superconductivity under pressure,

The phase diagram of recently discovered Fe based superconductors is quite similar (with some exceptions) to that of heavy fermions i.e. upon applying

chemical or external pressure, magnetism is suppressed and superconductivity emerges. FeSe_{1-x} is one of the above-mentioned exceptions: it does not exhibit static magnetic order for pressures up to about 30 GPa (300 kbar) [ME09] but short range spin fluctuations, strongly enhanced towards T_c [IM09]. μSR under pressure experiments [BE10] reveal that superconductivity is a bulk property and above 0.8 GPa (8 kbar) it coexists with magnetism with $T_N > T_c$. In a narrow pressure range, superconductivity competes with magnetism (the magnetic volume fraction and the magnetic order parameter are suppressed below T_c). A superconducting state coexisting with a phase-separated static magnetic order was observed by μSR under pressure in $(\text{Ba},\text{K})\text{Fe}_2\text{As}_2$, $(\text{Sr},\text{Na})\text{Fe}_2\text{As}_2$, and CaFe_2As_2 [GO09].

In the same context of trying to understand the complex phase diagram, magnetic and superconducting properties of the iron-based superconductors, μSR under pressure experiments on $\text{Fe}_{1.03}\text{Te}$ [BE12], which is an antiferromagnet at ambient pressure, have indicated a pressure induced ferromagnetism above 1.7 GPa, with a crossover region between the AF and F phases dominated by dynamical and incommensurate antiferromagnetism.

The phase diagrams of $\text{LaFeAsO}_{0.945}\text{F}_{0.055}$ and $\text{EuFe}_2(\text{As}_{1-x}\text{P}_x)_2$ were reconstructed by Khasanov et al. [KH11] and Guguchia et al. [GU12] from a combination of chemical/hydrostatic pressure investigations using μSR and magnetization measurements. De Renzi et al. [RE12] have investigated the effect of external pressure on the magnetic properties of LnFeAsO ($\text{Ln} = \text{La}, \text{Ce}, \text{Pr}, \text{Sm}$).

Fundamental parameters describing the superconductive state i.e. the London penetration depth λ , the gap values Δ , superfluid density, ... can also be obtained from μSR experiments and their evolution can be followed as a function of temperature, magnetic field and hydrostatic pressure: FeSe_{1-x} [KH10], RbFe_2As_2 [SH12], $\text{YBa}_2\text{Cu}_3\text{O}_x$ [MA11a].

c) Other compounds.

The pressure effect on the magnetic transition temperature of double perovskites [CA08], investigation of the time-reversal symmetry breaking in superconducting skutterudites [MA10], reentrant quantum criticality [MU11], topologically frustrated spin glasses [TE12] and pressure effects on spin-gap systems [SU09] are other, but not the only, interesting modern topics where μSR under pressure method has been successfully applied.

5. Development of p-cells for μ SR experiments

As mentioned above, the main requirements for the success of a μ SR under pressure experiments are: large samples, hydrostatic conditions, low temperatures, the possibility of attaining high pressures and the possibility of several pressure changes without opening the p-cell. The latter one is important for calibration reasons: each opening of the p-cell leads to changes in the sample position/distribution inside the sample space and requires another time-consuming calibration. Unfortunately there is little or no correlation to the previous calibration if the physical properties of the sample have changed during the pressurization. In the following, the design of the p-cell, the materials used to build the p-cell and accessories, are presented.

a) Design.

Large samples and hydrostatic conditions require the use of piston-cylinder pressure cells which can be calculated using the theory of long cylinder [ER96] and/or computer simulations using finite elements analysis, see Figure 11 for an example (PSI-pressure cell, opened one side).

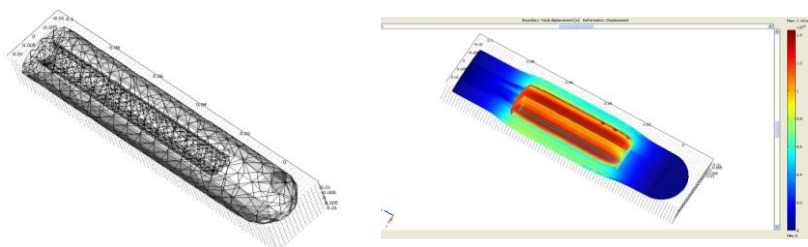


Figure 11. Simulation of the deformation of a p-cell, using the COMSOL software, in order to check the failure conditions. Deformations are exaggerated in the display.

When designing a pressure cell, several factors have to be taken into account. These include the size of the sample and/or inner diameter of the cryostat, amount of pressure needed (usually maximum of what the p-cell can support), ease of manipulation and last but not least, security.

When pressing a liquid with a piston in a cylindrical p-cell, there is some “chance” that liquid will leak from the cell under pressure because of small differences between the piston diameter and the inner diameter of the p-

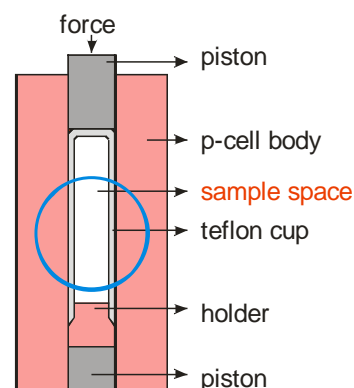


Figure 12. Usual sealing of a piston - cylinder pressure cell.

cell. Usually, leakage of piston-cylinder p-cells is prevented by using a simple system: the sample is placed inside a teflon container (teflon cup) filled with liquid and the applied pressure “seals“ the container by squeezing it on the bottom piece (the teflon cup holder), see Figure 12. Even though it provides a leak-proof system, the teflon cup has a “bad” μ SR signal with at least three components [AN01] and should not be placed in front of the beam (the blue circle).

In order to avoid this problem, two methods of sealing the p-cell have been employed: an adapted [AN01] type of sealing, Figure 13, for the p-cells opened one side or a mushroom type of sealing (Figure 14) for the p-cells opened both sides.

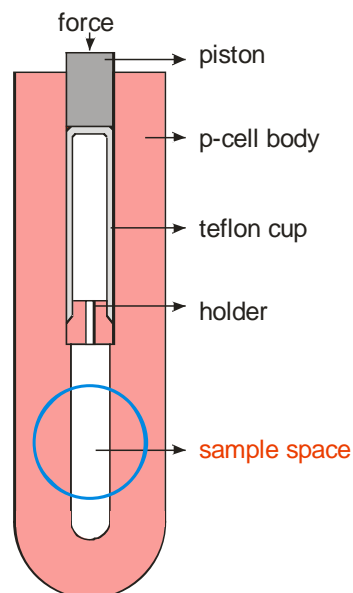


Figure 13. Adapted sealing for the PSI p-cell.

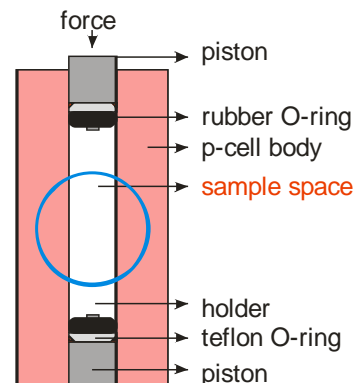


Figure 14. Mushroom-type of sealing.

The advantage of the p-cell opened one side compared with the p-cell opened both sides is that after being closed, one can increase/decrease several times the pressure without leakage. The disadvantages are: the length of the cylinder is bigger (larger deformation at the same pressure); the removal of the sample is sometimes difficult when the piston blocks; the sample space diameter is smaller than that of the piston.

In order to increase the limit of the pressure (see Figure 15) for the existent single layer (monobloc) pressure-cells the double layer design has been chosen for both types of p-cells (opened one side and opened both sides), with an external/internal diameter ratio exceeding 3. One way to produce two layer p-cells, is to taper the inside and outside cylinders and force them into each other with a press. The residual stresses at the interface add to the working stresses under pressure, and are thus partially cancelled.

The steps for producing the p-cells are presented in Figure 16. The tapered cylinders (can be produced by almost any well equipped machine-shop), are aged hardened at corresponding temperatures. Then, they are squeezed together using several tonnes force using a hydraulic press. The force needed to place the two cylinders in position depends strongly on the flatness of the two conical surfaces. Finally, the inner dimension of the sample and piston space are machined to the final dimension and polished. The finishing of the piston space is crucial for the good functioning of the pressure cell because quite a huge amount of friction can

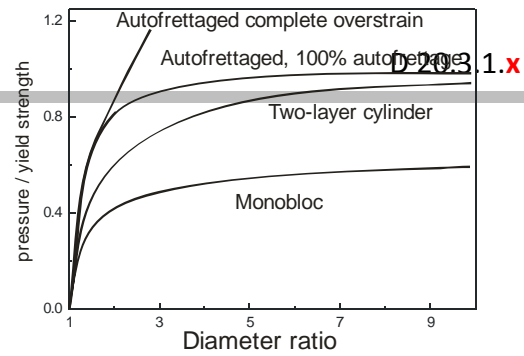


Figure 15. Maximum theoretical elastic pressure limits in terms of the yield strength of the materials, as a function of external/internal diameter ratio [DA70].

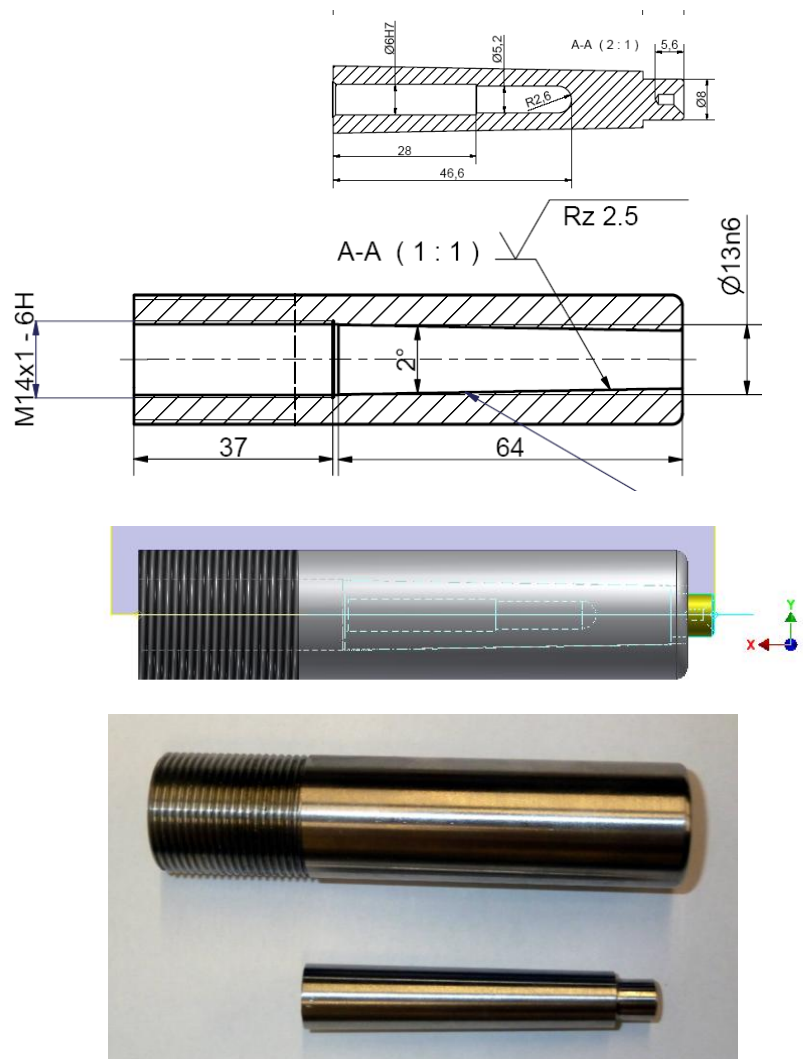


Figure 16. Design of the two layer p-cells (opened one end).

The finishing of the piston space is crucial for the good functioning of the pressure cell because quite a huge amount of friction can

develop between the sliding parts of the sealing system and the walls of the pressure cell, reducing the maximum pressure that one can get at the sample.

The same procedure is also employed for the pressure cell opened both sides. Figure 17 presents a picture of the sealing system for the p-cell opened one side while in Figure 18, a schematic view of the p-cell opened both sides is presented, together with a picture of the p-cell and the sealing system (only the left side mushroom sealing is shown here).



Figure 17. Picture of the sealing system for the p-cell opened one side.

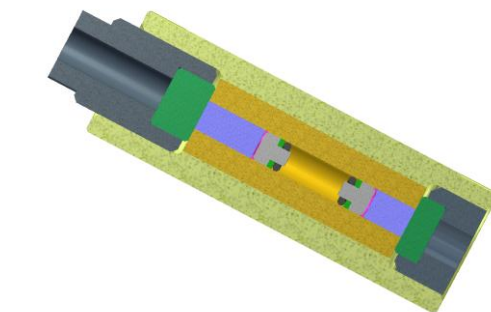


Figure 18. Up: Schematic view of the two-layer p-cell opened both side; Down: picture of the sealing system.

b) Materials

Taking into account that the materials are required to operate at high pressures, but also in magnetic fields, the critical requirement for their use in the building of pressure cells is that the disturbance to the magnetic field is negligibly small and that the materials retain no remnant magnetism after exposure. Nonmagnetic (or magnetically transparent) materials have to be employed for the built of the p-cell body, pistons, sealing elements and liquid for transmitting pressure.

Body of the p-cell is subjected to large tensile stresses. The “classical” Cu-Be and MP35N materials have been used to build the parts of the body of the p-cell. This is because of their strength but also because of their “easy to fit” contribution to the μ SR spectra.

CuBe25 is a nonmagnetic alloy down to, at least, 300 mK. There are several grades of Cu-Be with different mechanical properties. We have selected CuBe25 H grade, with a tensile strength of 800-980 GPa, before age hardening. The tensile strength is improved by age hardening and rises from about 1.35 GPa

at 293 K to 1.48 GPa at 20 K and the yield strength increases from 1.17 to 1.35 GPa over the same temperature interval [WA99]. Machining work hardened (but not age hardened) Cu-Be is not easy. Special care (cooling) has to be taken to avoid aging of the material during the machining process. This problem can be overcome by using a lead-doped Cu-Be alloy: small amount of lead promotes formation of finely divided chips thus extending cutting tool life [BR02] and providing an easy-to-machine alloy. After machining, the Cu-Be parts are heat treated for 2 hours at 315°C and then cooled in normal atmosphere.

Muons implanted in Cu-Be “see” only the magnetic field distribution (static) created by the nuclear magnetic moments and the corresponding μ SR spectra can be easily fitted with a so-called Kubo-Toyabe depolarization function [AN01]:

$$P(t) = P_{KT}(t) = \frac{1}{3} + \frac{2}{3} (1 - \Delta^2 t^2) \exp\left(-\frac{\Delta^2 t^2}{2}\right),$$

where Δ/γ_μ is the width of the field distribution at the muon site. The depolarization is constant over a large temperature interval, from the lowest temperature up to about 100 K. After 100 K diffusion starts and spectra become more exponential.

MP35N is described in the technical sheets of the producers as a high tensile strength nonmagnetic alloy with composition 35% Co, 35% Ni, 20% Cr and 10% Mo. It obtains most of its strength from work hardening and the remainder from an ageing process [WA99]. The sample is nonmagnetic down to low temperatures, but its magnetic moment depends strongly on the applied field (see Figure 19). Muons implanted in MP35N will “see” both the static magnetic field distribution created by the nuclear magnetic moments (Δ) and the dynamic (λ) field distribution created by the electronic moments in the paramagnetic phase. The μ SR spectra are fitted by an exponentially damped Kubo-Toyabe depolarization function, $P_{KT}(t)\exp(-\lambda t)$ with a value of Δ similar with that of Cu-Be but with a λ having strong temperature dependence at low temperatures (Figure 20), below 1 K. λ is small down to 1 K then increases abruptly indicating that correlations start to build between the electronic moments, but without magnetic ordering down to 0.26 K. The knowledge of the $\lambda(T)$ for each individual p-cell is important because different parts of the MP35N rods, from which the p-cells were built, can have slightly different chemical compositions (or homogeneity). λ is also field dependent, so using an MP35N p-cell for Knight shift measurements (transverse field in respect to the initial muon momentum) is not an easy task since it requires both a beam calibration (the beam is deflected by the applied transverse field) and a good calibration of the p-cell signal in field.

A so-called Russian alloy, or its Japanese version (Japanese Russian alloy) alloy have tensile properties similar to those of MP35N but has a μ SR signal with a much faster depolarized (not shown here) and is therefore more difficult to disentangle from the signal of a sample in magnetic phase. Only a few test p-cells

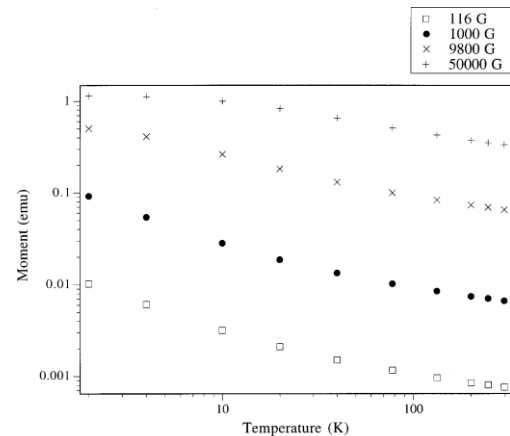


Figure 19. Magnetic moment of a 0.85 g sample of AMS 5844(E) MP35N sample in the age-hardened condition. Note the logarithmic axes [WA99].

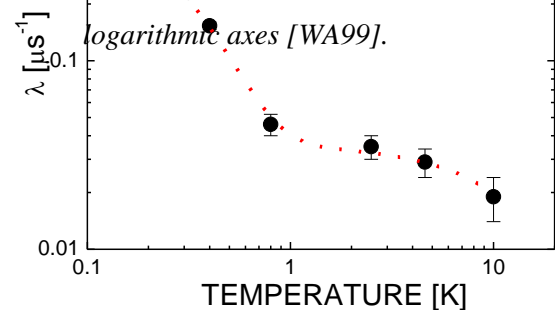


Figure 20. Temperature dependence of the relaxation rate λ for MP35N (logarithmic axes). λ increases abruptly below 1 K.

were built from this type of alloy. Moreover, these alloys are quite difficult to obtain.

Pistons are working in compression. They also have to be built from nonmagnetic materials (high speed steels are to be avoided). We are using pistons made out of tungsten carbide (K21) with the chemical composition Ni (10.5%) other (0.2%) WC (balance) having a compressive strength of 5100 MPa. They have a cylindrical shape with sharp edges. They are cut to the final dimensions by the manufacturer, with special care at respecting the tolerances and, most importantly, maintaining the 90 deg. angles between the active part and the sides of the pistons. Any deviation from the 90 deg. condition can lead to the chipping of the piston and its destruction/blockage following by the possible failure of the p-cell (see Figure 21).

Liquids for transmitting the pressure (LTP). Hydrostaticity at low temperature is the key ingredient of a liquid used as pressure transmitting media. There are a lot of LTP on the market: transformer oil / kerosene mixture, methanol / ethanol mixtures, 1:1 n-pentane / isoamyl alcohol, 1:1 mixture of Fluorinert FC70 and FC77, Daphne oil, to mention only the most widely used LTP's.

Among the above mentioned LTP's, the mixture of 1:1 n-pentane/isoamyl alcohol was shown to remain hydrostatic at room temperature to pressures greater than 30 kbar, Daphne oil 7373 to 20 kbar, 4:1 methanol/ethanol to 98 kbar, the Fluorinert mixture up to 8 kbar. If the pressure is changed when the LTP is still fluid, shear stresses will be small if the fluid solidifies when it is cooled. However, if pressure is applied to a solidified LTP significant shear stresses will be induced at low temperatures [BU09 and references therein].

We recommend the use of either the 1:1 mixture of n-pentane/isoamyl alcohol [BU09, WA99], or the Daphne oil [MU97]. Daphne oil is easier to manipulate both because it is more viscous and because it is less harmful, and

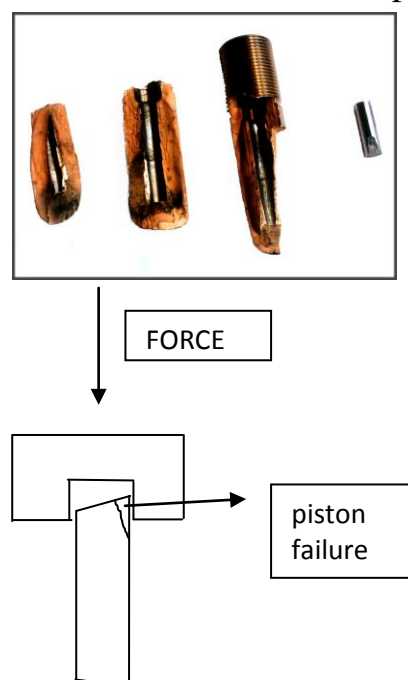


Figure 21. Failure of the piston and of the pressure-cell because of machining of the pistons (90 deg. condition not fulfilled).

therefore for low pressures it is a good choice. When hydrostaticity at higher pressures is needed, the alcohol mixtures are recommended but special care should be given to the preparation of the p-cells in order to avoid leakage (these mixtures have a low viscosity).

Applying and measuring the pressure. Pressure is applied at room temperature using a hydraulic press, Fig. 22. We usually go quite fast at the beginning (the first 4-5 kbar) in order to “clamp” the cell and avoid leakage, and then smoothly up to the desired pressure. The cell’s nut is tightened each 3-4 kbar.

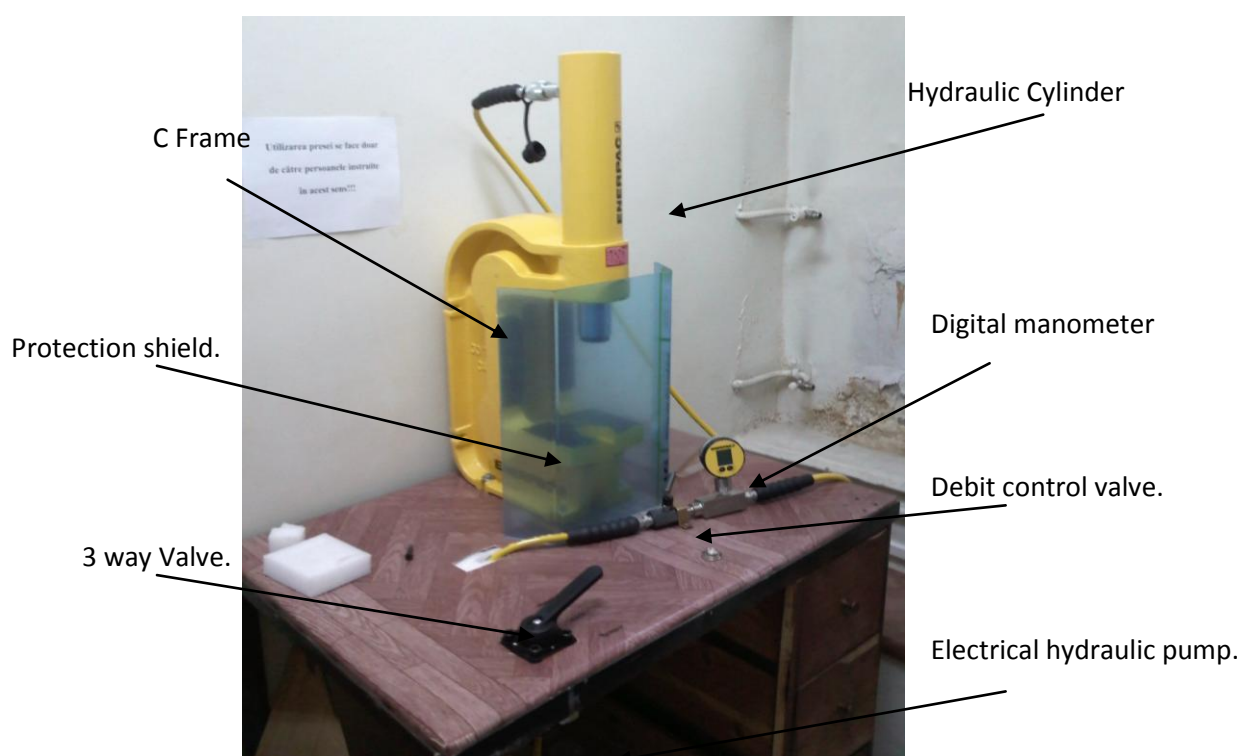


Figure 22. Picture of the hydraulic press (PSI and BBU).

With a good approximation, one needs about 10 kg force / mm² for each kbar. For a 6 mm diameter p-cell (approx 28 mm²) one needs about 280 kg force / kbar i.e. several tones for high pressures. Special care should be taken when applying pressure to any noise coming from the p-cell, since this might suggest chipping/blockage of the piston, unusual friction or irreversible damage to the p-cell. In such a situation one should immediately stop applying pressure and, if possible, release smoothly the pressure.

The displacement of the piston should also be carefully monitored. Firstly, at low pressures if the piston advances without a change in the applied pressure (3

way valve on “hold”) a leakage has occurred and one has to take a fast decision: either release the pressure, remove the cell, unload and prepare it again or, if the piston has not advanced too much, continue to increase the pressure hoping that the leak will be blocked. This last option should be selected only by experienced users because, if not stopped at the right moment, irreparable damage to the p-cell and possible to the sample might occur. Secondly, at high pressures, close to the limit of the p-cell, if the piston advances slowly but the monitored pressure does not change (3 way valve on “advance”) one should suspect that the elastic limit of the material was exceeded. In this case one should react very fast to slightly reduce the pressure, as otherwise the p-cell might break. Finally, if the pressure increases but the piston does not continue to advance, the piston has stuck inside the p-cell, either the piston is damaged or some dimensional limits were not taken correctly into account. In this case the pressure should be released and the problem should be investigated and solved.

Usually, a drop of several kbar expected from room temperature down to about 30 K because of the difference between the thermal expansion coefficients of CuBe (or MP35N) and that of the LTP. At high pressures this “natural” drop is increased by the effect of friction, which, in fact, seems to be the principal enemy of obtaining higher pressures in these large inner diameter pressure-cells.

Pressure is measured at low temperatures, either in situ (in the cryostat where the μ SR experiments are performed) or in a special dedicated glass cryostat, by monitoring the pressure dependence of the superconducting transition of a small piece of indium or lead placed inside the p-cell close to the sample. The measurement system is quite simple: A coil surrounding the p-cell (input coil) is fed with AC current. A second coil, under the first one, made up of two coils (one centered at the position of the manometer) wound in opposition are used as pick-up coils. The signal of the two pick-up coils is compensated above T_c but becomes uncompensated when the transition is crossed by lowering the temperature. The lack of compensation is evidenced by using a lock-in amplifier which compares the phase and amplitudes of the input signal with the pick-up signal.

References

[AN01] D. Andreica, Ph. D. Thesis, IPP/ETH-Zürich, (2001).

- [AM03] H. Amitsuka, K. Tenya, M. Yokoyama, A. Schenck, D. Andreica, F.N. Gygax, A. Amato, Y. Miyako, Ying Kai Huang and J.A. Mydosh, *Physica B* 326 (2003) 418.
- [AM04] A. Amato, M.J. Graf, A. deVisser, H. Amitsuka, D. Andreica and A. Schenck, *Journal of Physics:Condensed Matter* 16 (2004) S4403.
- [AM99] H. Amitsuka, M. Sato, N. Metoki, M. Yokoyama, K. Kuwahara, T. Sakakibara, H. Morimoto, S. Kawarazaki, Y. Miyako, and J. A. Mydosh, *Phys. Rev. Lett.* 83 (1999) 5114.
- [BE10] M. Bendele, A. Amato, K. Conder, M. Elender, H. Keller, H.-H. Klauss, H. Luetkens, E. Pomjakushina, A. Raselli, and R. Khasanov, *Phys. Rev. Lett.* 104 (2010) 087003
- [BE12] M. Bendele, A. Maisuradze, B. Roessli, S.N. Gvasaliya, E. Pomjakushina, S. Weyeneth, K. Conder, H. Keller, and R. Khasanov, arxiv.org/pdf/1209.0383.
- [BR02] Brush – Wellman, “Guide to Copper Beryllium”, 2002.
- [BU80] T. Butz, J. Chappert, J.F. Dufresne, O. Hartmann, E. Karlsson, B. Lindgren, L.O. Norlin, P. Podini and A. Yaouanc, *Phys. Lett. A* 75 (1980) 321.
- [BU86] T. Butz, G.M. Kalvius, B. Lindgren, O. Hartmann, R. Wäppling and E. Karlsson, *Hyp. Interact.* 32 (1986) 881.
- [BR-87] C. Broholm, et al., *Phys. Rev. Lett.* 58 (1987) 1467.
- [CA08] D. Di Castro, P. Dore, R. Khasanov, H. Keller, P. Mahadevan, Sugata Ray, D.D. Sarma, and P. Postorino, *Phys. Rev B* 78 (2008) 184416.
- [CO05] P. Coleman and J. Schofield, *Nature (London)* 433 (2005) 226.
- [DA70] T.E. Davidson and D.P. Kendall (1970), “The design of high pressure containers and associated equipment”, in *Mechanical behavior of materials under pressure* (ed. H.L.I.D.F. Pugh), 54-118, Elsevier, Amsterdam.
- [DE79] A.B. Denison, H. Graf, W. Kündig and P.F. Meier, *Helv. Phys. Acta* 52 (1979) 460.
- [DO-77] S. Doniach, *Physica (Amsterdam)* 91B (1977) 231.
- [EG12] N. Egetenmeyer, J. L. Gavilano, A. Maisuradze, S. Gerber, D. E. MacLaughlin, G. Seyfarth, D. Andreica, A. Desilets-Benoit, A.D. Bianchi, Ch. Baines, R. Khasanov, Z. Fisk and M. Kenzelmann, *Phys. Rev. Lett.* 108 (2012) 177204.

- [ER96] M. I. Eremets, “High Pressure Experimental Methods”, Oxford University Press, 1996.
- [GA57] R.L. Garwin, L.M. Lederman, and M. Weinrich, *Phys. Rev.* 105 (1957) 1415.
- [GE08] P. Gegenwart, Q. Si, and F. Steglich, *Nature Phys.* 4 (2008) 186.
- [GO09] T. Goko, A.A. Aczel, E. Baggio-Saitovitch, S.L. Bud’ko, P.C. Canfield, J.P. Carlo, G.F. Chen, Pengcheng Dai, A.C. Hamann, W.Z. Hu, H. Kageyama, G.M. Luke, J.L. Luo, B. Nachumi, N. Ni, D. Reznik, D.R. Sanchez-Candela, A.T. Savici, K.J. Sikes, N.L. Wang, C.R. Wiebe, T.J. Williams, T. Yamamoto, W. Yu, and Y.J. Uemura, *Phys. Rev. B* 80 (2009) 024508.
- [GU12] Z. Guguchia, A. Shengelaya, A. Maisuradze, L. Howald, Z. Bukowski, M. Chikovani, H. Luetkens, S. Katrych, J. Karpinski, and H. Keller, arxiv.org/pdf/1205.0212
- [HA94] O. Hartmann, E. Karlsson, R. Wäppling, L. Asch, S. Henneberger, G.M. Kalvius, A. Kratzer, H.-H. Klauß, F.J. Litterst and M.A.C. De Melo, *Hyp. Interact.* 85 (1994) 251.
- [HE09] R.H. Heffner, T. Goko, D. Andreica, K. Ohishi, W. Higemoto, T.U. Ito, A. Amato, J. Spehling, H.H. Klauss, E.D. Bauer, J.D Thompson and Y.J. Uemura, *Journal of Physics: Conference Series* 225 (2010) 012011
- [HI09] W. Higemoto, K. Satoh, T.U. Ito, E. Yamamoto, Y. Haga, Y. Onuki and A. Maisuradze, experimental report LMU/PSI-20091461.
- [IM09] T. Imai, K. Ahilan, F.L. Ning, T.M. McQueen, and R.J. Cava, *Phys. Rev. Lett.* 102 (2009) 177005.
- [KA00] *Hyperfine Interactions* 128 (2000) 275.
- [KH10] R. Khasanov, M. Bendele, A. Amato, K. Conder, H. Keller, H.-H. Klauss, H. Luetkens, and E. Pomjakushina, *Phys. Rev. Lett.* 104 (2010) 087004.
- [KH11] R. Khasanov, S. Sanna, G. Prando, Z. Shermadini, M. Bendele, A. Amato, P. Carretta, R. De Renzi, J. Karpinski, S. Katrych, H. Luetkens, and N.D. Zhigadlo, *Phys. Rev. B* 84 (2011) 100501(R).
- [KI05] N. Kimura, K. Ito, K. Saitoh, Y. Umeda, H. Aoki, and T. Terashima, *Phys. Rev. Lett.* 95 (2005) 247004.
- [KI07] N. Kimura, Y. Muro, and H. Aoki, *J. Phys. Soc. Jpn.* 76 (2007) 051010.
- [KL00] H.H. Klauß, private communication.

- [KR94] Kratzer, A., K. Mutzbauer, S. Heuneberger, G.M. Kalvius, O. Hartmaun, R. Wäppling, H.H. Klauß, M.A.C. de Melo, E.J. Litterst and Th. Stämmler, *Hyperfine Interactions* 87 (1994) 1055.
- [LI97] B. Lindgren, O. Hartmann, E. Karlsson, R. Wäppling, A. Yaouanc, T. Butz, L. Asch and G.M. Kalvius, *J. Magn. Magn. Mater.* 67 (1987) 130.
- [MA10] A. Maisuradze, W. Schnelle, R. Khasanov, R. Gumeniuk, M. Nicklas, H. Rosner, A. Leithe-Jasper, Yu. Grin, A. Amato, and P. Thalmeier, *Phys. Rev. B* 82 (2010) 024524.
- [MA11] A. Amaisuradze (LMU of PSI), private communication.
- [MA11a] A. Maisuradze, A. Shengelaya, A. Amato, E. Pomjakushina, and H. Keller, *Phys. Rev. B* 84 (2011) 184523.
- [MA96] Martin, E.M., 1996, Diplom Thesis (Physics Department, Technical University Munich, Germany, unpublished).
- [MA00] Martin, E.M., E. Schreier, G.M. Kalvius, A. Kratzer, O. Hartmarm, R. Wäppling, D.R. Noakes, K. Krop, R. Ballou and J. Deportes, *Physica B* 289 (2000) 265.
- [ME-09] S. Medvedev, T.M. McQueen, I.A. Troyan, T. Palasyuk, M.I. Erements, R. J. Cava, S. Naghavi, F. Casper, V. Ksenofontov, G. Wortmann, and C. Felser, *Nature Mater.* 8 (2009) 630.
- [MU98] Y. Muro, D. Eom, N. Takeda, and M. Ishikawa, *J. Phys. Soc. Jpn.* 67 (1998) 3601.
- [MU07] Y. Muro, M. Ishikawa, K. Hirota, Z. Hiroi, N. Takeda, N. Kimura, and H. Aoki, *J. Phys. Soc. Jpn.* 76 (2007) 033706.
- [MU11] T. Muramatsu, T. Kanemasa, T. Kagayama, K. Shimizu, Y. Aoki, H. Sato, M. Giovannini, P. Bonville, V. Zlatic, I. Aviani, R. Khasanov, C. Rusu, A. Amato, K. Mydeen, M. Nicklas, H. Michor, and E. Bauer, *Phys. Rev. B* (2011) 180404(R)
- [PA85] T.T.M. Palstra, et al., *Phys. Rev. Lett.* 55 (1985) 2727; W. Schlabititz, et al., *Z. Phys. B* 62 (1986) 171; M.B. Maple, et al., *Phys. Rev. Lett.* 56 (1986) 185.
- [RE12] R. De Renzi, P. Bonfá, M. Mazzani, S. Sanna, G. Prando, P. Carretta, R. Khasanov, A. Amato, H. Luetkens, M. Bendele, F. Bernardini, S. Massidda, A. Palenzona, M. Tropeano and Maurizio Vignolo, *Supercond. Sci. Technol.* 25 (2012) 084009.

- [RO11] D. P. Rojas, J.I. Espeso, J. Rodríguez Fernández, J.C. Gómez Sal, C. Rusu, D. Andreica, R. Dudric, A. Amato, *Physical Review B* 84 (2011) 024403.
- [SA10] S. Sakarya, P.C.M. Gubbens, A. Yaouanc, P. Dalmas de Réotier, D. Andreica, A. Amato, U. Zimmermann, N.H. van Dijk, E. Brück, Y. Huang, and T. Gortenmulder, *Phys. Rev. B* 81 (2010) 024429.
- [SC97] Schreier, E., S. Heuneberger, EL Burghart, A. Kratzer, G.M. Kalvius, O. Hartmann, M. Ekström and R. Wäppling, *Hyperfine Interactions* 104 (1997) 311.
- [SC99] Schreier, E., 1999, Doctoral Thesis (Physics Department, Technical University Munich, Germany, unpublished).
- [SH12] Z. Shermadini, H. Luetkens, A. Maisuradze, R. Khasanov, Z. Bukowski, H.-H. Klauss, and A. Amato, arxiv.org/pdf/1209.4753
- [ST06] O. Stockert, D. Andreica, A. Amato, H.S. Jeevan, C. Geibel, F. Steglich, *Physica B* 374 (2006) 167.
- [SI10] Q. Si and F. Steglich, *Science* 329 (2010) 1161.
- [SU09] T. Suzuki, I. Watanabe, F. Yamada, Y. Ishii, K. Ohishi, Risdiana, T. Goto, and H. Tanaka, *Phys. Rev. B* 80 (2009) 064407.
- [TA10] Y. Tada, N. Kawakami, and S. Fujimoto, *Phys. Rev. B* 81 (2010) 104506
- [TE07] T. Terashima, Y. Takahide, T. Matsumoto, S. Uji, N. Kimura, H. Aoki, and H. Harima, *Phys. Rev. B* 76 (2007) 054506.
- [TE12] M.T.F. Telling, K.S. Knight, F.L. Pratt, A.J. Church, P.P. Deen, K.J. Ellis, I. Watanabe, and R. Cywinski, *Physical Review B* 85 (2012) 184416.
- [TH89] J.D. Thompson, Z. Fisk, and G.G. Lonzarich, *Physica B* 161 (1989) 317.
- [UE07] Y.J. Uemura et al., *Nat. Phys.* 3 (2007) 29.
- [VI09] A. de Visser, N.T. Huy, A. Gasparini, D. E. de Nijs, D. Andreica, C. Baines and A. Amato, *Phys. Rev. Lett.* 102 (2009) 167003.
- [WA86] E. Wäckelgård, O. Hartmann, E. Karlsson, R. Wäppling, L. Asch, G.M. Kalvius, J. Chappert and A. Yaouanc, *Hyp. Interact.* 31 (1986) 325.
- [WA99] I.R. Walker, *Review of Scientific Instruments* 70 (1999) 3402.
- [WI66] H.J. Williams, J.H. Wernick, R.C. Sherwood, and G.K. Wertheim, *J. Appl. Phys.* 37 (1966) 1256.
- [YU04] W. Yu, F. Zamborszky, J.D. Thompson, J.L. Sarrao, M.E. Torelli, Z. Fisk, and S. E. Brown, *Phys. Rev. Lett.* 92 (2004) 086403.

